Dense inorganic electrolyte particles as a lever to promote composite electrolyte conductivity.

James A. Isaac[1], Didier Devaux[1], Renaud Bouchet[1,#]

[1]Univ. Grenoble Alpes, Univ. Savoie Mont Blanc, CNRS, Grenoble INP, LEPMI, 38000 Grenoble, France

[#]Corresponding author: Renaud.bouchet@lepmi.grenoble-inp.fr

Keywords: Composite electrolytes, ionic conductivity, impedance spectroscopy, effective medium theory, solid-state electrolytes.

ABSTRACT

Solid state batteries are seen as a key for the development of safer and higher energy density batteries, by limiting flammability and enabling the use of the lithium metal anode, respectively. Composite polymer/ceramic electrolytes are a possible solution for their realisation, by benefitting from the combined mechanical properties of the polymer electrolyte and the thermal stability and high conductivity of the ceramic electrolyte. Here, we use different liquid electrolyte chemistries as models for the polymer electrolytes, and evaluate the effect of adding a variety of porous and dense ceramic electrolytes on the conductivity. All results can be modelled with the effective medium theory, allowing predictions to be made on electrolyte combinations. We unambiguously determine that highly conductive porous particles act as insulators in such systems, whereas dense particles act as conducting, thereby advancing our understanding of composite electrolyte conductivity.

Traditionally, liquid electrolytes (LEs) have been used for lithium ion batteries[1] due to their high conductivity and good wettability of electrodes, but are far from ideal in terms of safety due to their flammable nature. LEs inability to suppress dendrite formation (causing short circuits and fire hazards upon cycling) also prevents the use of Li metal, the holy grail of negative electrodes.[2,3] Consequently, there has been an increased drive towards using solid state electrolytes as these could both improve safety and suppress dendrite formation .[4,5]

There are two major classes of solid state electrolytes: polymers (SPE) and ceramics (CE). SPE are advantageous in terms of their soft mechanical properties promising low cost processing such as solvent-free extrusion, and intimate contact with electrodes. However, the low SPE conductivity hinder their practical application at room temperature.[6,7] CEs have greater ionic conductivity and thermal stability, but their shaping requires high temperature and/or pressure leading to brittle materials.[3,8–11] Intimate Li/ceramic interfaces are difficult to form and maintain during the volume change of lithium upon cycling (Li platting/striping), generating delamination and cell failure[12] and/or dendrite formation.[13] Composite electrolytes comprising of dispersing ceramic particles in a polymer matrix seems a promising compromise to benefit from the advantages of each.

Across the wealth of literature, results of dispersed ceramic-in-polymer systems are diverse, unexpected and inconsistent. Among dispersed polymer/garnet systems, the results obtained often show an increase in ionic conductivity upon ceramic addition typically with a maximum between 2 vol%[14–19] and 20 vol%[20] of ceramic, followed by a decrease upon further addition.[14,15,24–30,16–23] Among PEO/LLZO based systems, addition of the ceramic results in a

composite conductivity a factor of two[17] to four orders of magnitude[26] higher than the polymer matrix. Others simply observe a decrease in the conductivity of the composite compared to the neat SPE.[31] Dispersed NaSICON ceramics in polymer matrices also give mixed results, the most common being a maximum conductivity for 2 – 10 vol% NaSICON,[32–35] or at higher ceramic loadings of 35 - 50 vol% .[36,37] Results with a monotonous increase in conductivity upon NaSICON addition have also been obtained,[27,38] and even certain cases where the composite electrolyte has a higher conductivity than each of its components.[35,39] Evidently, the factors driving the conductivity of dispersed CEs in conducting organic matrices are not clear, and a physical description of the effective conductivity is thus highly desired. Importantly, the impact of the polymer electrolyte reactivity with the ceramic particles and the particle microstructure have been disregarded.

Here, we use a model system for composite electrolytes where ceramic particles (LATP, LAGP, LLTO, LLZO, LLZTaO) are dispersed into liquid electrolytes (PEG, PC or DMF laden with LiTFSI) to measure the effect of ceramic addition on the conductivity. LEs (*i.e.* visco-elastic electrolyte media which mimic the properties of melt polymers) were used instead of SPEs because after measuring the conductivity of the dispersion (composite electrolyte), the ceramic particles can be allowed to sediment and the conductivity of the supernatant liquid measured, ensuring that any changes to the conductivity upon addition of ceramic particles are due to the ceramic and not changes to the liquid phase (degradation, dissolution, Li^+/H^+ exchange, *etc*.). The whole data set has been perfectly fitted (including data corrected for reactive LE/CE combinations) using an effective medium theory based on the Maxwell equation[40]. The model gives access to the effective conductivity of the particles (either dense or porous agglomerates) in the dispersion, enabling the diagnosis of problems due to the

microstructure of the ceramic powders, but also allows the prediction of outcomes for combinations of polymer and ceramic electrolytes requiring knowledge of only the conductivity of the respective components and the ceramic microstructure (particle porosity).

To provide the theory behind our experiment, we briefly introduce the effective medium theory. The Maxwell equation (**Equation 1**)[40] predicts the effective conductivity of a system in which a homogeneously dispersed phase is present inside a continuous phase, and is valid for systems where there is no particle-particle interaction (*i. e.* the norm in a dilute case).

$$\frac{\sigma_{eff}}{\sigma^0} = \frac{2\sigma^0 + \sigma_p - 2(1-\varepsilon_{LE})(\sigma^0 - \sigma_p)}{2\sigma^0 + \sigma_p + (1-\varepsilon_{LE})(\sigma^0 - \sigma_p)} \qquad \text{Eq. 1}$$

The effective conductivity of the mixture (σ_{eff}) divided by the conductivity of the continuous phase (σ^0, *i.e.* the LE or SPE) is a function of the conductivity of the dispersed CE phase (σ_p) and the volume fraction of the continuous LE domain (ε_{LE}). ε_{LE} can be calculated by dividing the initial volume of the liquid electrolyte (V_{LE}) by the total volume of the composite ($V_p + V_{LE}$):

$$\varepsilon_{LE} = \frac{V_{LE}}{V_p + V_{LE}} \qquad \text{Eq. 2}$$

In **Equation 1**, as soon as $\sigma_p > \sigma^0$, σ_{eff} is higher than σ^0 and continuously increases with the vol% of the CE. Thus, one can expect a continuous improvement in the conductivity of composite upon ceramic addition, at least until particle interactions modify the mechanism.

In the case of a dispersion of porous particles (*i.e.* herein made by aggregation of dense grains) with a porosity ε_p, **Equation 1** has been previously modified[41] introducing an effective porous-particle conductivity ($\sigma_{p,eff}$) defined such that the aggregated grains and internal porosity are considered as an effective medium, resulting in a modified Maxwell **Equation 3** for porous particles.

$$\frac{\sigma_{eff}}{\sigma^0} = \frac{2\sigma^0 + \sigma_{p,eff} - 2(1-\varepsilon_{ext})(\sigma^0 - \sigma_{p,eff})}{2\sigma^0 + \sigma_{p,eff} + (1-\varepsilon_{ext})(\sigma^0 - \sigma_{p,eff})} \quad \text{Eq. 3}$$

ε_{LE}, ε_{ext} and ε_p are related such that:

$$\varepsilon_{LE} = \varepsilon_{ext} + \varepsilon_p(1-\varepsilon_{ext}) \quad \text{Eq. 4}$$

Importantly, $\sigma_{p,eff}$ contains contributions from both the solid phase (grains and grain boundaries) and the continuous phase present inside the pores of the aggregates, as well as any conductivity along the surface of the grains[26] (see **Figure 1**).

In this work, the Maxwell equation is applied to a whole series of dispersed conducting ceramic particles in different continuous liquid electrolyte phases, in order to benchmark different combinations of composite electrolytes. By simply measuring the conductivity of the LE and the effective conductivity of LE/CE composite after each addition of ceramic (σ_{eff}), the effective conductivity of the dispersed ceramic phase can be calculated as long as ε_p is known. The possible factors affecting σ_{eff} are shown in **Figure 1**.

SEM images of the ceramic powders are displayed in **Figure S1-3**. The microstructures of these commercial powders, with the exception of LATP-Tosh, are made up of primary grains that are either aggregated or partially sintered together to form a porous secondary particle. Granulometry (see **Figure S4**) also confirms that the microstructure of the powders (*i.e.* aggregation) is preserved when dispersed in a liquid. We therefore divide these powders into two classes: porous and non-porous CEs, with LATP-Tosh being the sole example of the latter.

Conductivity of composites with porous particles.

Figure 2 displays the normalized conductivities at 40°C, *i.e.* the effective conductivity (σ_{eff}) divided by the conductivity of the liquid electrolyte (σ^0) against ε_{LE}. All behave in the same way: the addition of porous CE into a LE results in $\sigma_{eff}/\sigma^0 < 1$, *i.e.* the effective conductivity decreases with ceramic addition. The experimental points mostly follow the theoretical curves (purple dotted line) of $\sigma_p = 0$ (see **Eq. 1**) demonstrating that the porous agglomerates behave similarly to dense isolating particles. All the properties are driven by the agglomerate porosity, and not by the intrinsic conductivity of the ceramic electrolytes (typically the order of 10^{-3} – 10^{-4} S.cm^{-1} at 40°C. This result is found to be similar whatever the powder and electrolyte nature: the same powder in two different LEs delivers the same result. These results are very general and should apply to polymer electrolytes.[27,31]

Furthermore, the evolution of the effective conductivity as a function of ε_{LE} is always monotonous in the range $0.9 < \varepsilon_{LE} < 1.0$ (*i.e.* 0 to 10 vol% CE), in contrast to several examples reported in the literature.[14–19,32–35] It is important to note that in the case of LLZO-Schott in PEG-240 (*i.e.* 240 g/mol), addition of the ceramic to the liquid electrolyte did result in an increase in conductivity along with a LE colour change from colourless to brown (see **Figure S5a**)

suggesting a reactivity/LE degradation. To exalt this effect LLZO-Schott was added to PEG with no salt (similarly to certain published results)[21,26], resulting in a gain in conductivity by of a factor of 6 (see **Figure S5b**). However, the conductivity of the liquid electrolyte measured (σ^0) after particle sedimentation increases even more than σ_{eff} (**Figure S5b**), demonstrating that the gain in conductivity of the composite can be assigned to an increase in LE conductivity. Such a result could explain non-monotonous behaviour observed in the literature: initial addition of the ceramic results in an increase in conductivity due to degradation of the polymer electrolyte, dissolution of impurities on the surface of the ceramic, H^+/Li^+ exchange *etc.*, while further addition results in a decrease in conductivity due to the addition of porous ceramic particles (see **Figure 2**). Therefore, the results displayed in **Figure 2** are all calibrated against σ^0 measured from the decanted liquid electrolyte after addition of ceramic leading to a homogeneous behaviour for the whole set of combinations.

To further understand these porous systems, the experimental effective conductivity of the dispersion can be fitted using the modified-Maxwell **Equation 3** with a fixed value of ε_{ext} determined from **Equation 4** using the particle porosity ε_p (determined by mercury porosimetry, see **Table S1**), and adjusting the only unknown that is the effective conductivity of the porous particles $\sigma_{p,eff}$. All fits (added as lines in **Figure 2**) are excellent with a correlation factor $\chi^2 >$ 0.99. The resulting values of $\sigma_{p,eff}$ obtained using liquid electrolytes at different LiTFSI concentrations are displayed in **Figure 3**, along with the measured values of the corresponding decanted liquid electrolytes and expected ceramic electrolyte values (grey domains).

Three key observations can be made from **Figure 4**: i) $\sigma_{p,eff}$ is always below that of σ^0, ii) $\sigma_{p,eff}$ is completely independent to that of the expected value of the ceramic and iii) $\sigma_{p,eff}$

and σ^0 are proportional (the data for $\sigma_{p,eff}$ and σ^0 are parallel, with only a slight deviation at the lowest concentration 1 mM). Extrapolation suggests that obtaining a conductivity of the composite electrolyte with porous particles that is higher than the SPE seems not possible (excluding polymer degradation *etc.*), having serious implications for use as composite electrolytes.

To understand the effective conductivity of the porous particles, a plot of $\sigma_{p,eff}/\sigma^0$ *vs.* ε_p is displayed in **Figure 4**. For comparison, the theoretical plot for porous isolating particles is also displayed, which can be derived from the conductivity of a non-conducting particle (**Equation 6**) dispersion,[41] combined with the definition of tortuosity, τ_p (**Equation 7**),[41,43] giving **Equation 8**. This set of equations has been verified experimentally in the case of aqueous dispersion of dense silica spheres[41,44]. Basically, the inverse of tortuosity can be understood as an efficiency factor of the porous structure, with sinuous paths and dead ends, versus the ionic flux.

$$\sigma_{p,eff} = \frac{\sigma^0 \varepsilon_p}{\tau_p} \qquad \text{Eq. 6}$$

$$\tau_p = 1 - 0.49\ln(\varepsilon_p) \qquad \text{Eq. 7}$$

$$\frac{\sigma_{p,eff}}{\sigma^0} = \frac{\varepsilon_p}{1 - 0.49\ln(\varepsilon_p)} \qquad \text{Eq. 8}$$

In **Figure 4**, the effective conductivity of the particle $\sigma_{p,eff}$ for the ceramic electrolytes is superimposed with the predicted tortuosity of non-conducting particle dispersion (**Eq. 7**), indicating that $\sigma_{p,eff}$ is solely due to the conductivity of the liquid electrolyte present in the pores of the ceramic particles, and that the conductivity of the walls of the ceramic electrolyte (*i.e.* the ceramic material itself, grain and grain boundary) have an apparent conductivity of zero. This result can be explained by considering that in an aggregate, the grain/grain interactions are point contacts and therefore highly resistive compared to the bulk of the material (typically about 2 orders of magnitude between a compressed powder and a sintered pellet).[45]

Generally, research groups have studied the effect of nano-structured material for use in composite electrolytes, which has pushed suppliers to reduce the grain size of the ceramic particles, and consequently tends to produce strongly aggregate particles. Therefore, it is difficult to find commercial samples of ceramic electrolyte powders made up of dense/isolated particles, and our sole example of such a powder is LATP-Tosh.

Conductivity of composites with dense particles.

The normalized conductivity *vs.* ε_{LE} for the composite LATP-Tosh dispersed in PEG-240 at different salt concentrations is displayed in **Figure 5a**. The conductivity of the composite electrolyte at 10 mM is higher than that of the initial LE. The effective conductivity increases in a monotonous fashion, and was measured up to 32 vol% CE (*i.e.* ε_{LE}= 0.68). No change in σ^0 or colour was observed after particle sedimentation.

To determine the conductivity of ceramic particles in these systems, the experimental results were fitted with the Maxwell **Equation 1** valid for the absence of particle porosity

($\varepsilon_p = 0$) with σ_p being the only variable. The results of the fits are added in **Figure 5a**, which are in excellent agreement with the experimental data even up to 32 vol% CE. The resulting $\sigma_p$values at different salt concentrations are displayed in **Figure 5b**, along with the measured conductivities of the LE phases, and the expected CE conductivity.

In contrast to porous particles (see **Figure 3**), the σ_p values of the non-porous LATP-Tosh are relatively constant between 10 mM and 0.9 M, and are superimposed with the LATP conductivity (around 5 $\times 10^{-4}$ S.cm^{-1}, see results on sintered pellets in **Figure S6**). This indicates that for dispersed systems, the effective medium theory based on the Maxwell equation is always valid and predicts the effective conductivity of the composite knowing the conductivity of each of the components, as well as their microstructure (porous (**Eq. 3**, with $\sigma_{p,eff}$ calculated using **Eq. 8**) or dense (**Eq. 1**)). It is worth noticing that there are no unknowns in the model when dense particles are used: all parameters measured independently (ε_{LE}, σ_p, σ^0) can be injected into the model giving predictions that are fully consistent with experimental results (see dotted lines in **Figure 5a** and **5c** and **Table S2** for parameters). Differences between fitted and imposed (*i.e.* independently measured) values are typically between 15 and 50% with the exception of LATP in PEG-1000 at 10 mM.

A value of $\frac{\sigma_{eff}}{\sigma^0} < 1$ for liquid electrolytes PEG-240 at salt concentrations 100 mM or above (see **Figure 5a**) can be simply explained by the fact that the conductivity of the LE is higher than the value for the conductivity of LATP CE,[42] so a decrease in conductivity is expected upon ceramic addition.

In the practical application of such composites in solid state batteries, the continuous phase is a polymer with a conductivity several orders of magnitude lower than PEG-240 at the same salt

concentration. LATP will therefore have a higher conductivity than the continuous phase (*i.e.* $\sigma^0 < \sigma_p$), and, according to the Maxwell **Equation 1**, in such situations addition of LATP to the continuous phase would result in an increase in σ_{eff}. To assess the validity of such a concept, experiments were performed in PEG-1000 (*i.e.* 1000 g/mol). Indeed, a liquid-based organic electrolyte of higher molar mass has a lower conductivity due to an increased viscosity.[46] The results are displayed in **Figure 5c**.

At a salt concentration of 100 mM in PEG-1000, adding LATP-Tosh leads to an increase in conductivity ($\frac{\sigma_{eff}}{\sigma^0} > 1$, see **Figure 5c**) because the conductivity of PEG-1000 at 100 mM is well below the LATP value (**Figure 5d**). As with the data from **Figure 5b**, the calculated σ_p displayed in **Figure 5d** is superimposed with the expected LATP conductivity value (see **Figure S6**) when the salt concentration is in the range of 100 mM to 1 M, confirming the validity of **Equation 1** for modelling such systems.

A rise in σ_p is observed at 10 mM, which may be due to surface effects. Indeed, the extent of the length of the double layer (space charge layer on the side of the liquid electrolyte, stabilizing the liquid electrolyte/ceramic interface) increases when the salt concentration decreases, leading to a higher charge concentration in a significantly large volume at the surface of the ceramic particles.[44,47] This may cause a localized conductivity that is far higher than that of the bulk electrolyte, so the ceramic particles appear to be more conductive. Conversely, at high salt concentrations, the double layer will concern such a small volume that surface effects will be negligible.

We have demonstrated dispersion of ceramic particles into visco-elastic media (liquid or melt polymer electrolyte) will result in the increase in conductivity of the composite electrolyte

with respect to the starting LE, providing that i) the ceramic conductivity is higher than that of the continuous phase, and ii) particles are dense with no aggregation (*i.e.* $\varepsilon_p = 0$). The Maxwell Equation can be used to predict the conductivity of the composite electrolytes, knowing the conductivity of each of the components. The normalised predictions (σ_{eff}/σ^0) are displayed in **Figure S7**. While we have demonstrated that the Maxwell equation is consistent with experimental data up to 32 vol% of ceramic, predicted values may deviate at higher ceramic loading where particle interactions predominate. At low ceramic loadings (< 20 vol%), large gains in conductivity should not be expected with respect to the conductivity of the continuous phase electrolyte (LE/SPE), with only a gain of a factor of 2 obtained at 20 vol% ceramic where the ceramic is infinitely more conducting than the LE/SPE. The gain rises to a factor of 4 at 50 % and a factor of 8 at 70 % ceramic loading. These predictions suggest that the order of magnitude for the conductivity of the composite is always limited by the conductivity of the continuous phase, so solid state (polymer/ceramic) composites must contain a polymer with a significantly high conductivity as to not limit the overall conductivity.

Below the percolation threshold of ceramic particles within a liquid or polymer medium, a model based on the effective medium theory allows the interpretation of all the experimental data. Addition of porous particles to a visco-elastic electrolyte results in a systematic decrease of conductivity, regardless of the electrolyte nature and salt concentration. This is a microstructural effect which leads to an effective conductivity of the aggregate only driven by its porosity. Ceramic grain/grain contacts are blocking (at least two orders of magnitude lower than the bulk) leading to an overall isolating solid structure. An increase in conductivity is only observed when

the electrolyte is degraded by the ceramic, *e.g.* PEG-240 with LLZO. In contrast, addition of dense ceramic particles results in an increase in conductivity of the composite, as long as the conductivity of the CE is higher than the LE. In the absence of other effects, these results open the path for a direct extrapolation to an optimised composite electrolyte.

At low concentration, some surface effects can be observed (where charge accumulation in the double layer is expected to play a strong role), however no enhancement from surface conductivity at high concentrations are evident. Local effects may arise in polymers due to chain interactions with ceramic particles,[48] which could alter the surface conduction properties around ceramic electrolyte with respect to the relatively low conductivity of the polymer matrix. Interestingly, no impact of the ionic charge transfer resistance[49] at the CE/LE interface has been observed, which suggests that this contribution is small in our systems.

ACKNOWLEDGMENTS

The authors would like to thank Bernard Simon from the SAFT company for the mercury porosimetry measurements.

The Agence de la Transition Ecologique (ADEME) is acknowledge for the funding through the project IDOLES N°1982C0016.

AUTHOR CONTRIBUTIONS STATEMENT

R. B. designed the study. J. A. I. collected the experimental data. Data analysis and interpretation were performed by J. A. I. with the help of R. B. and D. D. The manuscript was written by J. A. I., R. B. and D. D. All authors have given approval to the final version of the manuscript.

COMPETING INTERESTS STATEMENT

The authors declare no conflict of interest.

FIGURE LEGENDS/CAPTIONS

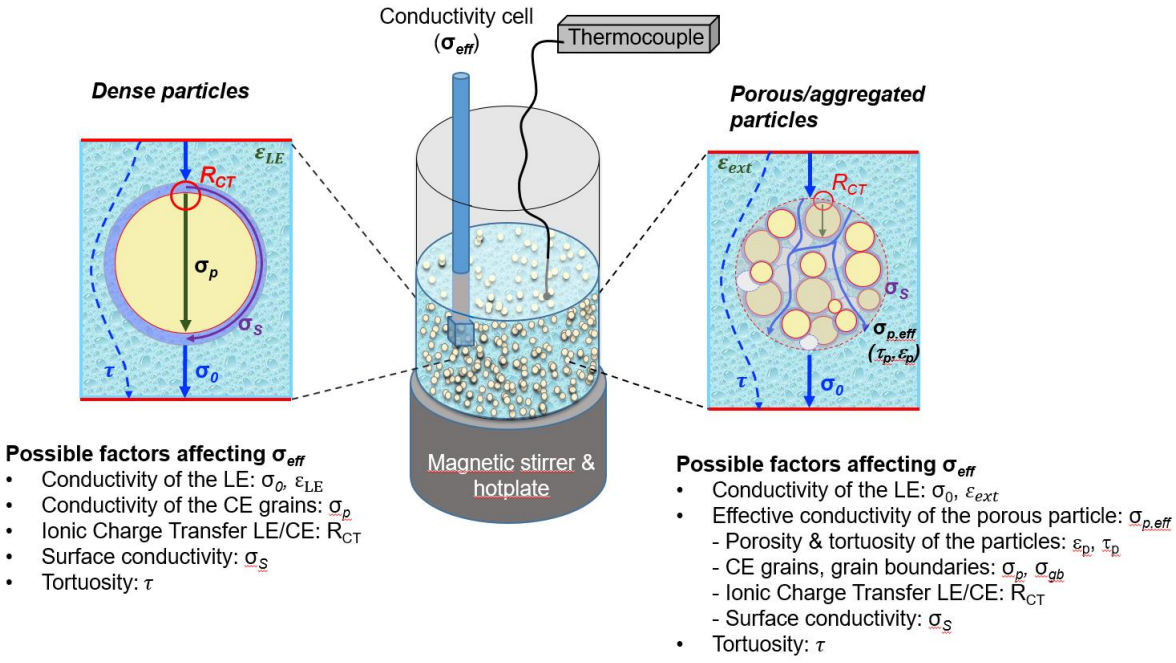


Figure 1: Possible factors that can affect the effective conductivity (σ_{eff}) of composite electrolytes. Comparison of dense and porous particles, in a system where a ceramic electrolyte is dispersed in a liquid electrolyte.

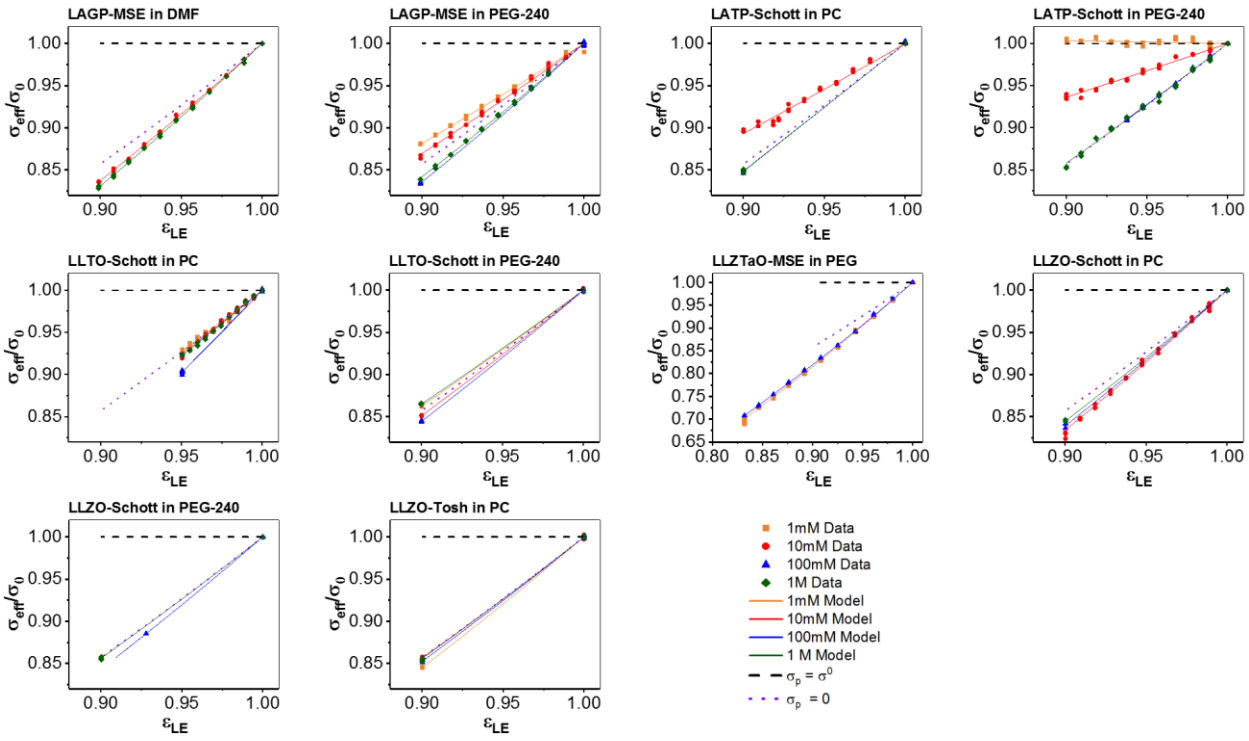


Figure 2: Conductivity of composites with porous particles. Normalized conductivity at 40°C of the composite σ_{eff}/σ^0 against liquid volume fraction (ε_{LE}) for different salt concentrations in the liquid electrolyte. Points: experimental data. Solid lines: fit results ($\chi^2 > 0.99$) using **Equation 3** where $\sigma_{p,eff}$ is the sole free parameter. Dotted lines: models using **Equation 1** for particles with bulk conductivity $\sigma_p = \sigma^0$ (black dashes) and $\sigma_p = 0$ (purple dots).

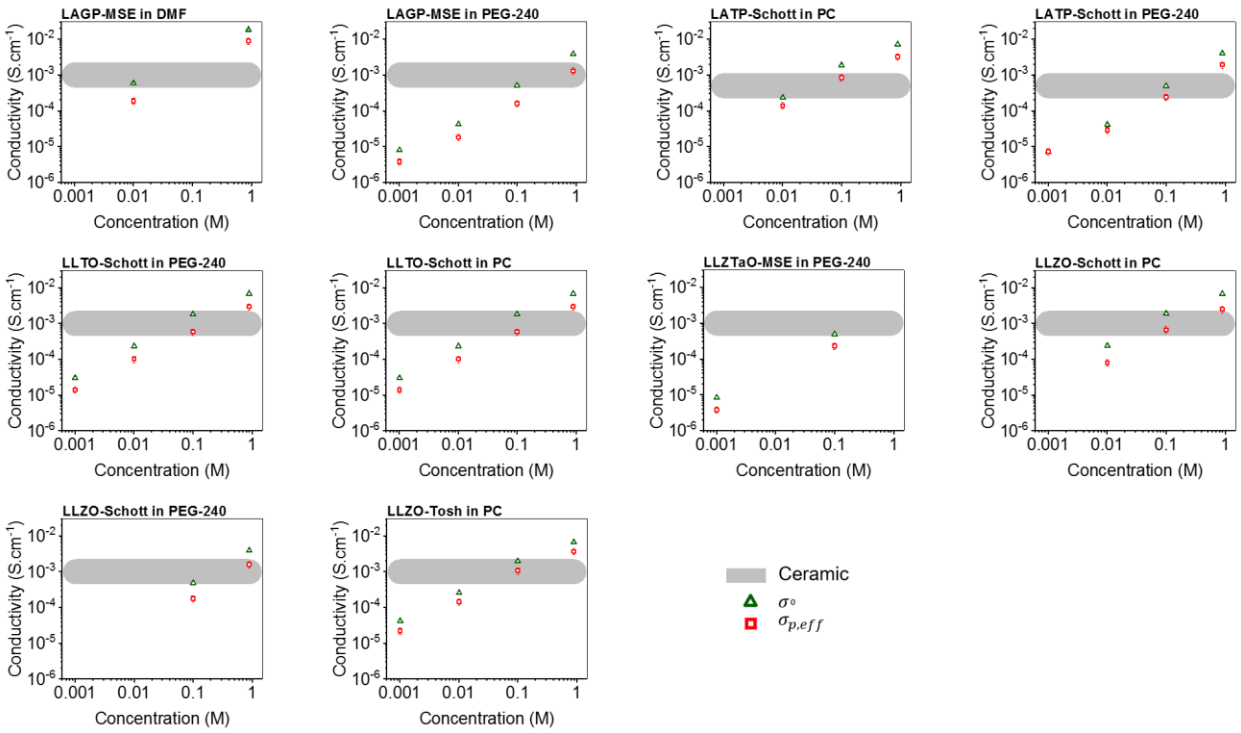


Figure 3: Effective conductivity of porous particles. The effective conductivities of the porous particles ($\sigma_{p,eff}$) are represented as red squares (with error bars representing the sensitivity to the parameter), the bulk liquid phase (σ^0, green triangles) and the expected ceramic electrolyte conductivity (grey band). $\sigma_{p,eff}$ was determined by fitting the data for the composite electrolytes displayed in **Figure 2** with the modified Maxwell **Equation 3**. Nominal ceramic conductivity values are 10^{-3} S.cm^{-1} for LLZO, LLTO and LAGP[42] and 5×10^{-4} for LATP (see **Figure S6**). All data at 40°C.

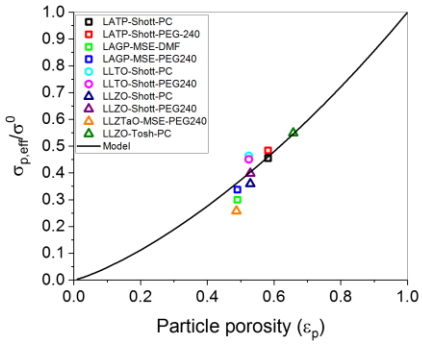


Figure 4: Modelling the conductivity of aggregated ceramic electrolyte particles as non-conducting. Effective conductivity of the porous particle divided by the conductivity of the liquid electrolyte ($\sigma_{p,eff}/\sigma^0$) against their porosity for all powders in liquid electrolytes, corresponding to the points at 1M LiTFSI from **Figure 3**. The solid line represents a dispersion of non-conducting particles (**Equation 8**).

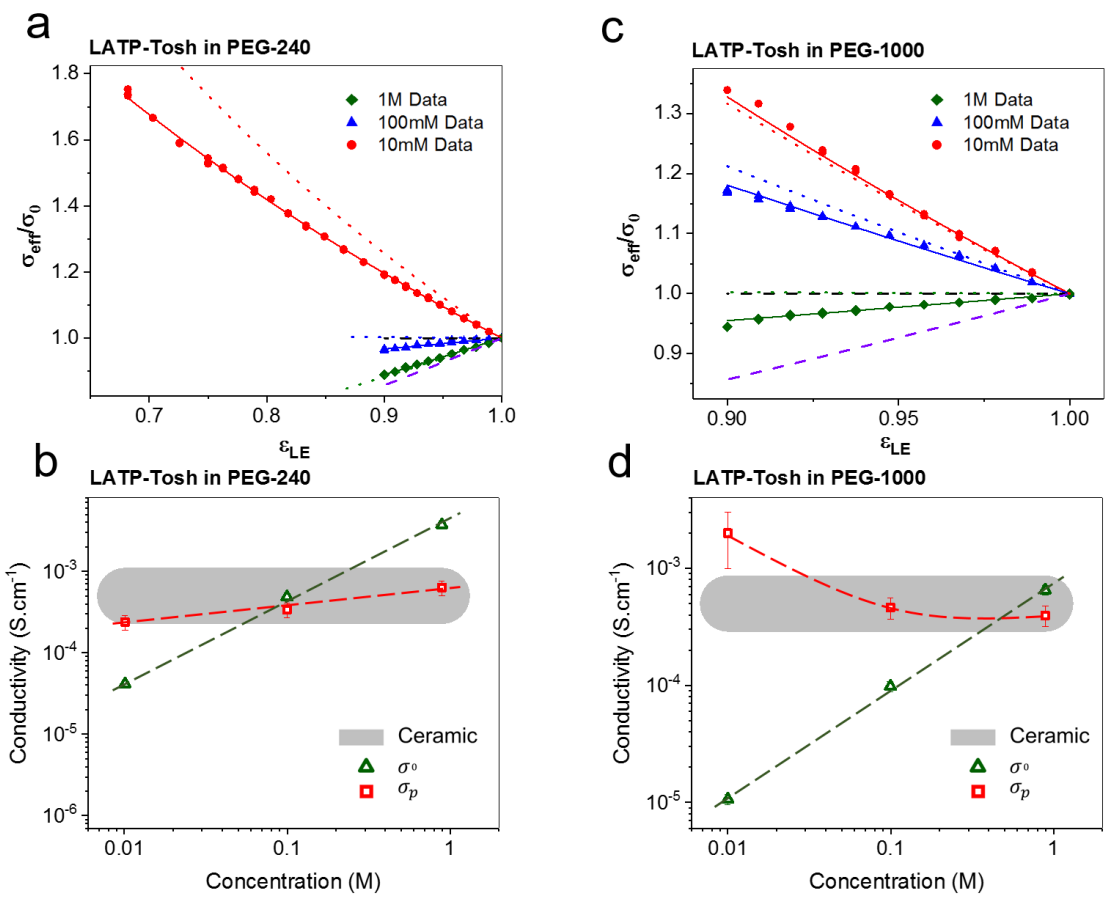


Figure 5: Conductivity of composites containing dense particles. Top: Normalized conductivity σ_{eff}/σ^0 of the composite electrolytes LATP-Tosh in PEG-240 at 40°C (**a**) and PEG-1000 at 46°C (**c**) at different concentrations of LiTFSI compared to ε_{LE}. Symbols represent experimental data, solid lines represent fits with **Equation 1** by using the experimental value of σ^0 and varying σ_p and dotted lines represent models using **Equation 1**, with σ^0 determined experimentally and σ_p fixed as the ceramic conductivity of 5 $\times 10^{-4}$ S.cm^{-1} and 7 $\times 10^{-4}$ S.cm^{-1} at 40°C and 46°C respectively (see **Figure S6** for LATP conductivity, along with Table S2 for model parameters). Dashed lines: models using **Equation 1** for particles with bulk conductivity $\sigma_p = \sigma^0$ (black) and $\sigma_p = 0$ (purple). Bottom: conductivity of the particle (σ_p) determined from the corresponding fits (with error bars representing the sensitivity to the parameter), along with

measured values of σ^0 and the expected typical value for the conductivity of LATP (see **Figure S6**) with PEG-240 at 40°C (**b**) and PEG-1000 at 46°C (**d**). The dashed lines in (**b**) and (**d**) are a guide to the eyes.

DATA AVAILABILITY

The data that support the findings of this study are available from the corresponding author upon reasonable request.

REFERENCES

(1) Armand, M.; Tarascon, J. M. Issues and Challenges Facing Rechargeable Lithium Batteries. *Nature* **2001**, *414* (6861), 359–367. https://doi.org/10.1038/35104644.

(2) Chu, S.; Cui, Y.; Liu, N. The Path towards Sustainable Energy. *Nat. Mater.* **2016**, *16* (1), 16–22. https://doi.org/10.1038/nmat4834.

(3) Varzi, A.; Raccichini, R.; Scrosati, B. Challenges and Prospects of the Role of Solid Electrolytes in the Revitalization of Lithium Metal Batteries. *J. Mater. Chem. A Mater. energy Sustain.* **2016**, *4*, 17251–17259. https://doi.org/10.1039/C6TA07384K.

(4) Tan, D. H. S.; Banerjee, A.; Chen, Z.; Meng, Y. S. From Nanoscale Interface Characterization to Sustainable Energy Storage Using All-Solid-State Batteries. *Nat. Nanotechnol.* **2020**. https://doi.org/10.1038/s41565-020-0657-x.

(5) Chen, R.; Li, Q.; Yu, X.; Chen, L.; Li, H. Approaching Practically Accessible Solid-State Batteries: Stability Issues Related to Solid Electrolytes and Interfaces. *Chem. Rev.* **2019**. https://doi.org/10.1021/acs.chemrev.9b00268.

(6) Long, L.; Wang, S.; Xiao, M.; Meng, Y. Polymer Electrolytes for Lithium Polymer Batteries. *J. Mater. Chem. A Mater. energy Sustain.* **2016**, *4*, 10038–10069. https://doi.org/10.1039/C6TA02621D.

(7) Zhou, D.; Shanmukaraj, D.; Tkacheva, A.; Armand, M.; Wang, G. Polymer Electrolytes for Lithium-Based Batteries: Advances and Prospects. *Chem* **2019**, *5* (9), 2326–2352. https://doi.org/10.1016/j.chempr.2019.05.009.

(8) Sun, C.; Liu, J.; Gong, Y.; Wilkinson, D. P.; Zhang, J. Recent Advances in All-Solid-State Rechargeable Lithium Batteries. *Nano Energy* **2017**, *33* (January), 363–386. https://doi.org/10.1016/j.nanoen.2017.01.028.

(9) Meesala, Y.; Jena, A.; Chang, H.; Liu, R. S. Recent Advancements in Li-Ion Conductors for All-Solid-State Li-Ion Batteries. *ACS Energy Lett.* **2017**, *2* (12), 2734–2751. https://doi.org/10.1021/acsenergylett.7b00849.

(10) Famprikis, T.; Canepa, P.; Dawson, J. A.; Islam, M. S.; Masquelier, C. Fundamentals of Inorganic Solid-State Electrolytes for Batteries. *Nat. Mater.* **2019**, *18* (12), 1278–1291. https://doi.org/10.1038/s41563-019-0431-3.

(11) Balaish, M.; Gonzalez-Rosillo, J. C.; Kim, K. J.; Zhu, Y.; Hood, Z. D.; Rupp, J. L. M. Processing Thin but Robust Electrolytes for Solid-State Batteries. *Nat. Energy* **2021**. https://doi.org/10.1038/s41560-020-00759-5.

(12) Lewis, J. A.; Cortes, F. J. Q.; Liu, Y.; Miers, J. C.; Verma, A.; Vishnugopi, B. S.; Tippens, J.; Prakash, D.; Marchese, T. S.; Han, S. Y.; et al. Linking Void and Interphase Evolution to Electrochemistry in Solid-State Batteries Using Operando X-Ray Tomography. *Nat.*

Mater. **2021**, *c*. https://doi.org/10.1038/s41563-020-00903-2.

(13) Kasemchainan, J.; Zekoll, S.; Spencer Jolly, D.; Ning, Z.; Hartley, G. O.; Marrow, J.; Bruce, P. G. Critical Stripping Current Leads to Dendrite Formation on Plating in Lithium Anode Solid Electrolyte Cells. *Nat. Mater.* **2019**, *18* (10), 1105–1111. https://doi.org/10.1038/s41563-019-0438-9.

(14) Zhang, J.; Zang, X.; Wen, H.; Dong, T.; Chai, J.; Li, Y.; Chen, B.; Zhao, J.; Dong, S.; Ma, J.; et al. High-Voltage and Free-Standing Poly(Propylene Carbonate)/Li6.75La3Zr1.75Ta0.25O12 Composite Solid Electrolyte for Wide Temperature Range and Flexible Solid Lithium Ion Battery. *J. Mater. Chem. A* **2017**, *5* (10), 4940–4948. https://doi.org/10.1039/c6ta10066j.

(15) Chen, F.; Yang, D.; Zha, W.; Zhu, B.; Zhang, Y.; Li, J.; Gu, Y.; Shen, Q.; Zhang, L.; Sadoway, D. R. Solid Polymer Electrolytes Incorporating Cubic Li7La3Zr2O12 for All-Solid-State Lithium Rechargeable Batteries. *Electrochim. Acta* **2017**, *258*, 1106–1114. https://doi.org/10.1016/j.electacta.2017.11.164.

(16) Zhang, X.; Liu, T.; Zhang, S.; Huang, X.; Xu, B.; Lin, Y.; Xu, B.; Li, L.; Nan, C. W.; Shen, Y. Synergistic Coupling between Li6.75La3Zr175Ta0.25O12 and Poly(Vinylidene Fluoride) Induces High Ionic Conductivity, Mechanical Strength, and Thermal Stability of Solid Composite Electrolytes. *J. Am. Chem. Soc.* **2017**, *139* (39), 13779–13785. https://doi.org/10.1021/jacs.7b06364.

(17) Chen, L.; Li, Y.; Li, S. P.; Fan, L. Z.; Nan, C. W.; Goodenough, J. B. PEO/Garnet Composite Electrolytes for Solid-State Lithium Batteries: From “Ceramic-in-Polymer” to

"Polymer-in-Ceramic." *Nano Energy* **2018**, *46* (August 2017), 176–184. https://doi.org/10.1016/j.nanoen.2017.12.037.

(18) Li, R.; Wu, D.; Yu, L.; Mei, Y.; Wang, L.; Li, H.; Hu, X. Unitized Configuration Design of Thermally Stable Composite Polymer Electrolyte for Lithium Batteries Capable of Working Over a Wide Range of Temperatures. *Adv. Eng. Mater.* **2019**, *21* (7). https://doi.org/10.1002/adem.201900055.

(19) Villa, A.; Verduzco, J. C.; Libera, J. A.; Marinero, E. E. Ionic Conductivity Optimization of Composite Polymer Electrolytes through Filler Particle Chemical Modification. *Ionics.* **2021**, *27*, 2483–2493. https://doi.org/10.1007/s11581-021-04042-9.

(20) Zha, W.; Chen, F.; Yang, D.; Shen, Q.; Zhang, L. High-Performance Li6.4La3Zr1.4Ta0.6O12/Poly(Ethylene Oxide)/Succinonitrile Composite Electrolyte for Solid-State Lithium Batteries. *J. Power Sources* **2018**, *397* (July), 87–94. https://doi.org/10.1016/j.jpowsour.2018.07.005.

(21) Zhang, J.; Zhao, N.; Zhang, M.; Li, Y.; Chu, P. K.; Guo, X.; Di, Z.; Wang, X.; Li, H. Flexible and Ion-Conducting Membrane Electrolytes for Solid-State Lithium Batteries: Dispersion of Garnet Nanoparticles in Insulating Polyethylene Oxide. *Nano Energy* **2016**, *28*, 447–454. https://doi.org/10.1016/j.nanoen.2016.09.002.

(22) Zhao, C. Z.; Zhang, X. Q.; Cheng, X. B.; Zhang, R.; Xu, R.; Chen, P. Y.; Peng, H. J.; Huang, J. Q.; Zhang, Q. An Anion-Immobilized Composite Electrolyte for Dendrite-Free Lithium Metal Anodes. *Proc. Natl. Acad. Sci. U. S. A.* **2017**, *114* (42), 11069–11074. https://doi.org/10.1073/pnas.1708489114.

(23) Cheng, S. H. S.; He, K. Q.; Liu, Y.; Zha, J. W.; Kamruzzaman, M.; Ma, R. L. W.; Dang, Z. M.; Li, R. K. Y.; Chung, C. Y. Electrochemical Performance of All-Solid-State Lithium Batteries Using Inorganic Lithium Garnets Particulate Reinforced PEO/LiClO4 Electrolyte. *Electrochim. Acta* **2017**, *253*, 430–438. https://doi.org/10.1016/j.electacta.2017.08.162.

(24) Tao, X.; Liu, Y.; Liu, W.; Zhou, G.; Zhao, J.; Lin, D.; Zu, C.; Sheng, O.; Zhang, W.; Lee, H. W.; et al. Solid-State Lithium-Sulfur Batteries Operated at 37 °C with Composites of Nanostructured Li7La3Zr2O12/Carbon Foam and Polymer. *Nano Lett.* **2017**, *17* (5), 2967–2972. https://doi.org/10.1021/acs.nanolett.7b00221.

(25) Liang, Y. F.; Deng, S. J.; Xia, Y.; Wang, X. L.; Xia, X. H.; Wu, J. B.; Gu, C. D.; Tu, J. P. A Superior Composite Gel Polymer Electrolyte of Li7La3Zr2O12- Poly(Vinylidene Fluoride-Hexafluoropropylene) (PVDF-HFP) for Rechargeable Solid-State Lithium Ion Batteries. *Mater. Res. Bull.* **2018**, *102* (March), 412–417. https://doi.org/10.1016/j.materresbull.2018.02.051.

(26) Li, Z.; Huang, H. M.; Zhu, J. K.; Wu, J. F.; Yang, H.; Wei, L.; Guo, X. Ionic Conduction in Composite Polymer Electrolytes: Case of PEO:Ga-LLZO Composites. *ACS Appl. Mater. Interfaces* **2019**, *11* (1), 784–791. https://doi.org/10.1021/acsami.8b17279.

(27) Samsinger, R. F.; Schopf, S. O.; Schuhmacher, J.; Treis, P.; Schneider, M.; Roters, A.; Kwade, A. Influence of the Processing on the Ionic Conductivity of Solid-State Hybrid Electrolytes Based on Glass-Ceramic Particles Dispersed in PEO with LiTFSI. *J. Electrochem. Soc.* **2020**, *167* (12), 120538. https://doi.org/10.1149/1945-7111/abb37f.

(28) Mei, X.; Wu, Y.; Gao, Y.; Zhu, Y.; Bo, S. H.; Guo, Y. A Quantitative Correlation between Macromolecular Crystallinity and Ionic Conductivity in Polymer-Ceramic Composite Solid Electrolytes. *Mater. Today Commun.* **2020**, *24* (February), 101004. https://doi.org/10.1016/j.mtcomm.2020.101004.

(29) Kamaya, N.; Homma, K.; Yamakawa, Y.; Hirayama, M.; Kanno, R.; Yonemura, M.; Kamiyama, T.; Kato, Y.; Hama, S.; Kawamoto, K.; et al. A Lithium Superionic Conductor. *Nat. Mater.* **2011**, *10* (9), 682–686. https://doi.org/10.1038/nmat3066.

(30) Kato, M.; Hiraoka, K.; Seki, S. Investigation of the Ionic Conduction Mechanism of Polyether/Li 7 La 3 Zr 2 O 12 Composite Solid Electrolytes by Electrochemical Impedance Spectroscopy. *J. Electrochem. Soc.* **2020**, *167* (7), 070559. https://doi.org/10.1149/1945-7111/ab8478.

(31) Langer, F.; Bardenhagen, I.; Glenneberg, J.; Kun, R. Microstructure and Temperature Dependent Lithium Ion Transport of Ceramic-Polymer Composite Electrolyte for Solid-State Lithium Ion Batteries Based on Garnet-Type Li7La3Zr2O12. *Solid State Ionics* **2016**, *291*, 8–13. https://doi.org/10.1016/j.ssi.2016.04.014.

(32) Wang, Y. J.; Pan, Y.; Kim, D. Conductivity Studies on Ceramic Li1.3Al0.3Ti1.7(PO4) 3-Filled PEO-Based Solid Composite Polymer Electrolytes. *J. Power Sources* **2006**, *159* (1 SPEC. ISS.), 690–701. https://doi.org/10.1016/j.jpowsour.2005.10.104.

(33) Zhao, Y.; Huang, Z.; Chen, S.; Chen, B.; Yang, J.; Zhang, Q.; Ding, F.; Chen, Y.; Xu, X. A Promising PEO/LAGP Hybrid Electrolyte Prepared by a Simple Method for All-Solid-State Lithium Batteries. *Solid State Ionics* **2016**, *295*, 65–71.

https://doi.org/10.1016/j.ssi.2016.07.013.

(34) Xia, Y.; Wang, X.; Xia, X.; Xu, R.; Zhang, S.; Wu, J.; Liang, Y.; Gu, C.; Tu, J. A Newly Designed Composite Gel Polymer Electrolyte Based on Poly(Vinylidene Fluoride-Hexafluoropropylene) (PVDF-HFP) for Enhanced Solid-State Lithium-Sulfur Batteries. *Chem. - A Eur. J.* **2017**, *23* (60), 15203–15209. https://doi.org/10.1002/chem.201703464.

(35) Wang, W.; Yi, E.; Fici, A. J.; Laine, R. M.; Kieffer, J. Lithium Ion Conducting Poly(Ethylene Oxide)-Based Solid Electrolytes Containing Active or Passive Ceramic Nanoparticles. *J. Phys. Chem. C* **2017**, *121* (5), 2563–2573. https://doi.org/10.1021/acs.jpcc.6b11136.

(36) Jung, Y.-C.; Lee, S.-M.; Choi, J.-H.; Jang, S. S.; Kim, D.-W. All Solid-State Lithium Batteries Assembled with Hybrid Solid Electrolytes. *J. Electrochem. Soc.* **2015**, *162* (4), A704–A710. https://doi.org/10.1149/2.0731504jes.

(37) Park, M. S.; Jung, Y. C.; Kim, D. W. Hybrid Solid Electrolytes Composed of Poly(1,4-Butylene Adipate) and Lithium Aluminum Germanium Phosphate for All-Solid-State Li/LiNi0.6Co0.2Mn0.2O2 Cells. *Solid State Ionics* **2018**, *315* (December 2017), 65–70. https://doi.org/10.1016/j.ssi.2017.12.007.

(38) MacFarlane, D. R.; Newman, P. J.; Nairn, K. M.; Forsyth, M. Lithium-Ion Conducting Ceramic/Polyether Composites. *Electrochim. Acta* **1998**, *43* (10–11), 1333–1337. https://doi.org/10.1016/S0013-4686(97)10039-1.

(39) Yi, J.; Liu, Y.; Qiao, Y.; He, P.; Zhou, H. Boosting the Cycle Life of Li-O2 Batteries at Elevated Temperature by Employing a Hybrid Polymer-Ceramic Solid Electrolyte. *ACS*

Energy Lett. **2017**, *2* (6), 1378–1384. https://doi.org/10.1021/acsenergylett.7b00292.

(40) Maxwell, J. C. *A Treatise on Electricity and Magnetism*; Clarendon Press: Oxford, 1873; Vol. 1.

(41) Barrande, M.; Bouchet, R.; Denoyel, R. Tortuosity of Porous Particles. *Anal. Chem.* **2007**, *79* (23), 9115–9121. https://doi.org/10.1021/ac071377r.

(42) Hou, M.; Liang, F.; Chen, K.; Dai, Y.; Xue, D. Challenges and Perspectives of NASICON-Type Solid Electrolytes for All-Solid-State Lithium Batteries. *Nanotechnology* **2020**, *31* (13), 132003. https://doi.org/10.1088/1361-6528/ab5be7.

(43) Weissberg, H. L. Effective Diffusion Coefficient in Porous Media. *J. Appl. Phys.* **1963**, *34* (9), 2636–2639. https://doi.org/10.1063/1.1729783.

(44) Bouchet, R.; Devaux, D.; Wernert, V.; Denoyel, R. Separation of Bulk, Surface, and Topological Contributions to the Conductivity of Suspensions of Porous Particles. *J. Phys. Chem. C* **2012**, *116* (8), 5090–5096. https://doi.org/10.1021/jp210614h.

(45) Kubanska, A.; Castro, L.; Tortet, L.; Schäf, O.; Dollé, M.; Bouchet, R. Elaboration of Controlled Size Li1.5Al0.5Ge1.5(PO4)3 Crystallites from Glass-Ceramics. *Solid State Ionics* **2014**, *266*, 44–50. https://doi.org/10.1016/j.ssi.2014.07.013.

(46) Devaux, D.; Bouchet, R.; Glé, D.; Denoyel, R. Mechanism of Ion Transport in PEO/LiTFSI Complexes: Effect of Temperature, Molecular Weight and End Groups. *Solid State Ionics* **2012**, *227*, 119–127. https://doi.org/10.1016/j.ssi.2012.09.020.

(47) Pfaffenhuber, C.; Göbel, M.; Popovic, J.; Maier, J. Soggy-Sand Electrolytes: Status and

Perspectives. *Phys. Chem. Chem. Phys.* **2013**, *15* (42), 18318–18335. https://doi.org/10.1039/c3cp53124d.

(48) Aveyard, R.; Bijsterbosch, B. H.; Cosgrove, T.; Goodwin, J. W.; Gregory, J.; Greiser, F.; Healy, T. W.; Lovelock, B.; Lyklema, J.; Ottewill, R. H.; et al. *Solid/Liquid Dispersions*; Tadros, T. F., Ed.; Academic Press Inc. (London) Ltd., 1987.

(49) Weiss, M.; Simon, F. J.; Busche, M. R.; Nakamura, T.; Schröder, D.; Richter, F. H.; Janek, J. From Liquid - to Solid - State Batteries : Ion Transfer Kinetics of Heteroionic Interfaces. *Electrochem. Energy Rev.* **2020**, No. 0123456789. https://doi.org/10.1007/s41918-020-00062-7.

METHODS

Ceramics LATP-Schott, LLTO-Schott and LLZO-Schott were purchased from Schott, LAGP-MSE and LLZTaO-MSE were purchased from MSE supplier, LLZO-Tosh and LATP-Tosh were obtained from Toshima Manufacturing Co., Ltd.. Anhydrous Propylene carbonate (PC) and dimethylformamide (DMF) were purchased from Sigma Aldrich, and polyethylene glycol dimethyl ether with an average molecular weights of 240 $g.mol^{-1}$ (PEG-240) and 1000 $g.mol^{-1}$ (PEG-1000) were purchased from TCI chemicals and Sigma Aldrich respectively. LiTFSI was purchased from Solvay. All products were immediately stored in a Jacomex argon filled glove box (O_2, H_2O <1 ppm) and used as received.

The microstructures of the ceramic powders were analyzed by SEM using a Zeiss Ultra 55. Granulometry of each ceramic powder was performed dispersing (with an ultrasonic finger)

the powder in ethanol and measuring using a Mastersizer 3.0 to ensure that the aggregation seen in SEM imaging are representative of the powder microstructure in the dispersion. The porosity of each of the powders was measured by mercury porosimetry measurements using a Autopore IV from Micromeritics, where 1g of powder was introduced into the penetrometer 10.0554 (designed for powder).

To prevent any moisture pollution, all the conductivity measurements were made in the glove box. The procedure was previously developed in the context of the dispersion of dense non-conducting glass beads, where the experimental results perfectly matched the predictions with the Maxwell Equation.[41] 7 ml of the liquid electrolyte with LiTFSI concentration varying between 1 mM and 1 M was placed in a vial on a hot plate to regulate the temperature at 40°C (with the exception of PEG-1000 at which a temperature of 46°C was used to ensure a molten state), and successive amounts of ceramic powder were added (generally up to 10% volume). The suspension was stirred at 1000 RPM to ensure that the ceramic powder was homogeneously dispersed in the liquid electrolyte. Impedance measurements were obtained after each addition of ceramic using a VPM300 purchased from BioLogic by placing a two pole immersion conductivity cell made of platinized platinum electrodes (CDC479, Radiometer Analytical) into the stirred suspension. At the end of the experiment, the particles in the composite were allowed to settle, and the liquid electrolyte was decanted and re-measured to ensure that any changes to the conductivity of the composite upon ceramic addition were due to the presence of ceramic particles only, and not to an evolution of the liquid electrolyte conductivity. Only in the case of addition of LLZO-Schott to PEG-240 did such an evolution occur. Measurements and reproducibility were also made by taking the composite electrolyte at the lowest salt concentration and adding salt (to obtain a value at a higher salt concentration), re-measuring the

conductivity of the composite then decanting the liquid electrolyte and measuring its conductivity. Frictional interactions can be considered as negligible, since i) the conductivity of the composite is independent of the rotation rate (see **Figure S8**) as long as the rate is high enough to homogeneously disperse the particles and ii) all results were consistent with the Maxwell Equation independent of the particle size, salt concentration and liquid viscosity (which would all alter frictional interactions). The temperature was measured by placing a thermocouple (Farnell) into the suspension before and after the measurement of each impedance spectrum to ensure a fluctuation of less than 0.1 °C. The impedance spectra were modelled using the software Z-view (Scribner Inc.) using an equivalence circuit of a resistance and an inductance in series (representing the cables), a resistance in parallel with a constant phase element (CPE) representing the electrolyte, followed by a CPE to model the blocking platinum electrode/electrolyte interface. Measured resistances were reproducible with an error typically less than 0.2 %. The conductivity was then determined by dividing the cell constant for the microelectrode (obtained by measuring the resistance of a 0.1 M solution of KCl) by the measured resistance of the electrolyte.

The volume of ceramic particles added (V_p) was determined by dividing the total mass of the particles added (m_p) by the density of the ceramic material (ρ) (see SI for details).

$$V_p = \frac{m_p}{\rho} \qquad \text{Eq. 9}$$